Resarch on Microstructure and Property of Zirconium alloy in the Rotary forging process by GNN-FEM

Yong Gao *, Xiaobo Li, Qiang Yue, Weishan Duan, Xiangjun Li, Xiangfeng Ji

C State Nuclear Bao Ti ZirconiumIndustry Company, Baoji Shannxi China, 721013

* Corresponding Author Email: harry_3005@163.com

Abstract. In this paper, the effect of resarch on rotary forging process of Zirconium alloy bar was studied by combining Metallographic observation, electron microscope observation, Convolutional neural networks (CNN) and finite element (FEM). The results show that Point pits and scratches often occur in rotary forging. Modifying die size and increasing entrance Angle can effectively improve such defects as point pits and scratches. The external structure of Zirconium alloy bar is relatively dense, and the internal structure is relatively loose. The number and size of micro-holes after acid erosion are small. The number and size of the tiny holes after internal acid erosion are large. The (0002) planes of the inner and outer grains of the Zirconium alloy bar are basically parallel to the rolling direction, but the outer (0002) is concentrated on the pole, and the inner (0002) pole is approximately distributed in a ring around the longitudinal axis. As a result, there are differences in the small holes inside and outside the bar after corrosion The effect of resarch on the classification Method of RF in by GNN, which the Accuracy-Avg is 96%. At the beginning of RF, the rolled pass exerts compressive stress on the outside of the Zirconium alloy bar, and the outside of the bar is the first to undergo plastic deformation. With the increase of RE deformation, the bar strain gradually increases and is gradually transferred from the outside to the inside. The effect of resarch on the classification Method of by GNN-FEM is an efficient and convenient method to simulate the microstructure and stress distribution of zirconium alloy in the process of RF.

Keywords: Zr allay, RF, GNN, FEM classification, Metallographic observation, Electron microscope observation.

1. Introduction

Zirconium alloy is an excellence property, a better thermal neutron cross section absorption and tensile strength at high temperatures and pressures, were used for Cladding tube and structural material in the nuclear reactor. End plug is a structural material, which is sealeding cladding tube for preventing nuclear (UO2) proliferation. The principle of rotary forging is to use three or more high-speed rotating molds to forge the material, so as to achieve changes in the size of the material, which is a branch of precision forging, the process has high deformation efficiency, fast speed, high precision, so it is widely used in the material processing industry. At present, rotary forging is mainly used in cemented carbide and rare metals, and the corresponding literature reports are as follows: Qingle Meng studied that according to the actual processing situation, the factors causing hollow break in thick molybdenum wires are overall analyzed in the respect of molybdenum density, impurity composition, processing and etc. The main contributing factors are forging technology as external factor and impurity composition as internal factor. The countermeasures and controlling essentials are provided, which has great significance to guide molybdenum wire processing. Ming Luo researched that The Mo-Ti-Zr alloy rods were prepared by cold isostatic pressing, high temperature sintering and direct rotary forging. The effects of the annealing temperature on the mechanical properties and microstructure of the alloy and the annealing behavior of this rotary forging Mo-Ti-Zr alloy rods deformed by 30% were investigated. The results show that, with increasing annealing temperature before 1 000℃, the hardness of the Mo-Ti-Zr alloy rods decreases slowly whereas the tensile strength and elongation increase. The tensile strength and elongation reach 669 MPa and 3.1%, respectively, at 900℃.The recrystallization of the Mo-Ti-Zr alloy rods occurs and the grains are refined at the annealing temperature of 800−1 000℃. For the rotary forging Mo-Ti-Zr alloy rods, its fracture is mainly a transcrystalline fracture type. The mixed type of transcrystalline fracture and

intergranular fracture in the refined grains increases with increasing annealing temperature. Wei Hang studied The microstructure evolution and properties of Cu-0.51Cr-0.06Zr alloy under processeing of rotary forging and heat treatment were investigated by means of SEM, EDS, TEM, HRTEM. The results show that the Cr-rich dendritic phases in the microstructure of as-cast Cu-0.51Cr-0.66Zr alloy is spheroidized into particles or rods after hot forging, the long rodd-shaped Cr-rich phase with a larger size is about 5 μm, the particle-shaped and short rod-shaped Cr-rich phases with a smaller size are less than 1 μm, and the distribution of these Cr - rich phases shows a certain directionality with the direction of rotary forging deformation. In addition, during aging process, the precipitated nano -scale phases is identified to be body centered cubic structure and their sizes are 4-7 nm. The tensile strength and conductivity of the as-cast alloy after rotary forging, aging and final rotary forging are 625 Mpa, 82.7%IACS, repectively [1-5]. At present, there is convolutional neural network (CNN) is a kind of simulation method commonly used in material processing industry. In this paper, there is a way to resarch on microstructure and property of Zirconium alloy in the Rotary forging (RF) process by GNN, and for The study on the hot rotary forging process of Zirconium alloy provides theoretical and practical significance [6-8]. In this paper, present, the finished zirconium rod is enlarged (200X) after corrosion, and a corrosion pit structure can be observed on the inner and outer surfaces of the zirconium rod. In this paper, the causes are studied and simulation analysis is carried out by using GNN-FEM, which provides theoretical and practical significance for ensuring the safety of nuclear components and nuclear reactors.

2. Methodology

2.1. RF

RF is a kind of radial processing technology. When tow, four or even more than Six equivalent molds rotate around the axis of the bar blank, high-frequency strikes are made along its radial direction, so that the billet is compressed and deformed along the axis by radial force, and the deformation process of the external surface of the bar blank from "round to non-round to round" occurs, as shown in Figure 1. Thus the purpose of rotary forging is realized. It is a kind of long axis, local and continuous, chip free, precision metal processing technology.

Generally, there are two basic forging methods in rotary forging process: one is the "feed forging method", in which the forging die rotates around the blank and makes a short stroke and high frequency of hammering along the radial direction. In this process, the blank is fed directly from the die inlet until the desired forging length is reached or all of it passes through the die. This method is suitable for forging unilateral step shaft or long straight shaft, the step transition cone feed Angle is small, the maximum is not more than 20°; The other is called "concave forging method". In addition to rotating forging around the billet and short stroke and high frequency hammering on the billet, the mold can also be "opened" and "closed". This method is suitable for forging two-way steps and intermediate reduction processing technology, and the step transition at both ends is short and steep, such as the processing of automobile crankshaft.

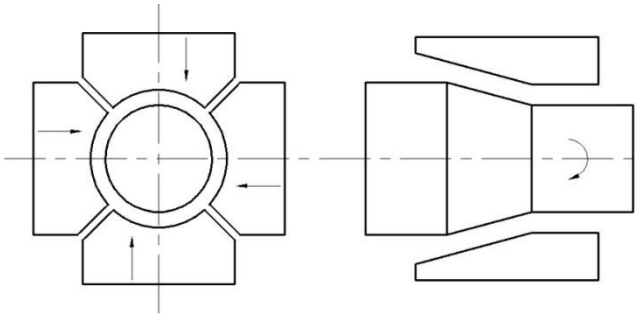

(a) Working principal diagram

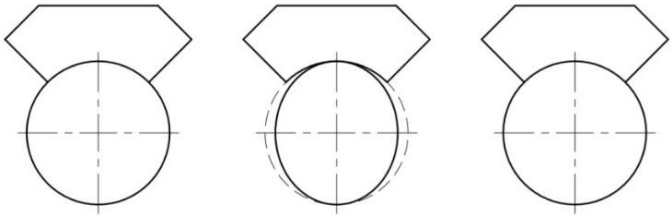

(b) Deformation diagram

Figure 1. Deformation and Working principal diagram of RF for the Zr alloy

The dimensional accuracy, surface quality and mechanical properties of the workpiece after rotary forging mainly depend on the flow direction of metal materials in the process of rotary forging. In addition to the influence of its own fluidity, the metal flow direction mainly depends on the structural parameters and profile design of the rotary forging die. The design of rotary forging die mainly involves the following parameters:

(1) Design parameters of die outlet and inlet chamfer: the inlet chamfer is too large, the vibration is large during feeding, and the rod billet end is easy to bump with the inner surface of the chamfer, resulting in burrs, curling and other phenomena, affecting the surface quality and dimensional accuracy; The inlet chamfer is too small, which is not conducive to the initial feeding; The large chamfer shortens the effective length of the sizing section, reduces the sizing time, and affects the surface quality of the bar after rotary forging. The chamfer is too small to cause secondary damage to the fully formed bar material, such as scratches, bruises, and other defects;

(2) Lateral effective clearance of the die: buffer and absorb the radial counteracting force of the bar blank on the inner surface of the die and the metal flow in this direction during the rotary forging process. When the clearance is too large, the metal radial flow along the cross section increases, and the phenomenon of "ribbing" becomes more obvious. Because the clearance is too small, the radial flow of metal along the cross section of the bar is limited, so the counteracting force on the die surface increases, and it is easy to crack and damage under the action of high frequency pulse.

(3) Mold cone feeding Angle: the Angle design is too large, according to the force analysis during feeding, it can be seen that the metal flow acting on the axial reverse increases, resulting in increased resistance to rod feeding, which is not conducive to controlling surface quality and dimensional accuracy, and reduce production efficiency; If the Angle design is too small, the metal flow momentum along the axial direction decreases, while the flow momentum along the axial and radial direction increases. Under the buffering and absorption of the lateral effective gap, the phenomenon of "edging" is easy to occur. When the Angle is close to 0°, the two ends of the bar blank are easy to form stepped defects. In addition, with the increase of radial flow, the force acting on the inner surface of the mold increases, and the high frequency pulse impact force of the mold is enhanced, which is easy to crack and damage.

(4) Mold profile and cavity ellipticity: This parameter has the same effect as the lateral effective clearance.

(5) The zirconium rod after rotational forging has been corroded and enlarged (200X), and the surface morphology of the zirconium rod inside and outside is inconsistent.

2.2. GNN-FEM

A deep learning algorithm primarily used to process data with a grid-like structure, such as images and speech signals. The convolutional neural network extracts features and classifies them through components such as convolutional layer, pooling layer and fully connected layer. The GNN (Convolutional neural network) structure is shown in Fig 2.

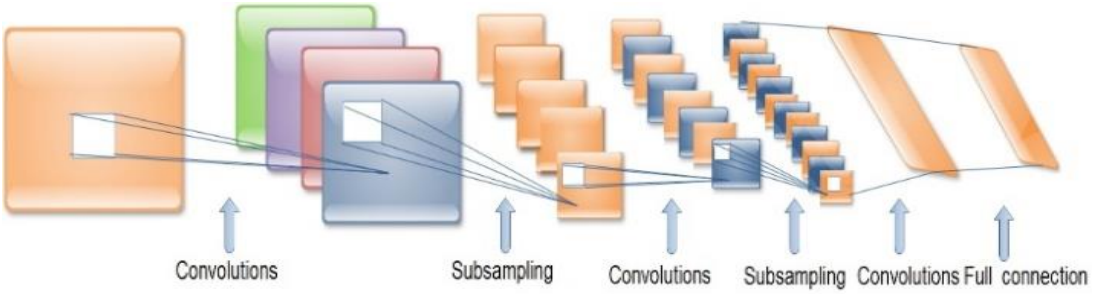

Figure 2. GNN structure

GNN is a kind of neural network, it has the characteristics of fast speed and high calculation effect, completely abandons the disadvantages of Artificial neural network(ANN) and falling into the local minimum, and can be higher than the accuracy of Support Vector Machine (SVM) network, so a wide range of materials processing, mechanical manufacturing, electrical design and other professional has been widely used Experimental. SVM was first created by Vapnik based on structural risk minimization in statistical theory, with the idea of creating a categorical hyperplane as a decision surface to maximize the edge of isolation between positive and negative examples while ANN is a network structure model that fits the input and output results directly.

To prevent the accuracy of image acquisition, preventing other external noise from affecting image acquisition, the 3D laser scanner Artec3D EVA placed the maps shards cleaned by dust on the surface on a rotating tray during the collection process to conduct 3D laser scanning and collect the 3D model of the shards. The model obtained by scanning may have noise due to illumination, repeated scanning, and other reasons, resulting in feature loss and affecting the experimental results. The built-in software of the EVA laser scanner manually de-noises the scanning results, which Accuracy-Avg defined as follows:

$$\text{Accuracy} - \text{Avg} = \sqrt{\frac{1}{N}\sum_{i=1}^{N}(T_i - Y_i)^2} \quad (1)$$

Where N is the number of training or testing data, i is the number of variables in the output, Ti and Yi is the target output and network output for neuron i, respectively.

Based on the finite element method (FEM) and theory, a theoretical model of rotary forging of Zirconium alloy bar was established to analyze the strain trend distribution of Zirconium alloy bar during external and internal processing.

3. Experimental Data

3.1. Experimental material

The Experimental material ϕ 22 mm bar billet, the main chemical composition of Zirconium alloy alloy is: W (Sn) is 1.2% ~ 1.7%, w (Fe) is 0.18% ~ 0.24%, w (Cr) is 0.06% ~ 0.13%, w (C) < 0.027%, w (H) is 0.0025%, w (O) is 0.16% and contains some special elements, the matrix for Zr.

3.2. Experimental facilities

(1) Metallographic observation equipment

The sample size is 20mm×20mm×30mm. The samples were roughed to fine with 200#, 400#, 800#, 1000# and 1200# sandpaper in sequence on the automatic polishing machine, and were

mechanically polished with 0.05μm SiO2 polishing paste. The etching agent with acid ratio of hydrofluoric acid: nitric acid: water = 3:5:12 was used to etch the end face, and the metallographic sample was prepared. The microstructures of the samples were observed under an inverted Zeiss research grade VertA1 microscope.

(2) Structure detection

The annealed sample of each finished product is first polished with water sandpaper, then mechanically polished, and then vibrationally polished with a vibratory polishing machine. After polishing, the sample is pickled with a mixture of H2SO4, HNO3 and HF. After the sample was prepared, SEM EBSD technology was used to analyze the texture of the outside and inside of the sample.

(3) Simulation

By using the method and theory of finite element and numerical analysis, the theoretical model of rotary forging of Zirconium alloy bar was established to analyze the strain trend distribution of Zirconium alloy bar during external and internal processing.

3.3. Experiment parameter

The model selected on site is C7116-2ZF cold rotary forging machine for processing Zirconium alloy rods. The equipment is small in size, easy to install, adjust and operate, has low requirements on operating environment, low price of spare parts, and low operation and maintenance cost. The maximum processing diameter of the equipment is 25mm, the minimum diameter is 5mm, and the dimensional accuracy is ±0.15mm. The microstructure and texture of outer and inner Zirconium alloy bar after spinning forging were observed, and the process of spinning forging was simulated.

4. Results and discussion

(1) Experimental result

The surface "ribbing" of the rotary forged bar is obvious, the diameter and size of the bar fluctuates greatly, and the removal amount needs to be increased in the subsequent core-less grinding and polishing processes, thus increasing the workload. In addition, part of the bar is scrapped due to local abnormal size, especially for the Zirconium alloy bar, the economic loss is large, as shown in Fig 3, resulting in poor quality of the outer circular surface; rotary forging 132 rods were selected as test samples, and the test results were shown in Table 1. Most of the sizes were off the upper or lower limit, and the size distribution was relatively discrete, which indicated that the size fluctuated greatly during the rotary forging process of Zirconium alloy rods, and the consistency of processing sizes was poor, which increased the removal amount and workload of the subsequent coarseness grinding process, and increased the rod material loss. According to statistics, Zirconium alloy rod should be more than 2-5mm grinding off the thickness of the rod, that is, according to the calculation of 200 pieces of material per batch, each batch of rotary forging material will consume Zirconium alloy rod, especially for the rare and expensive material H rod, the economic loss is larger.

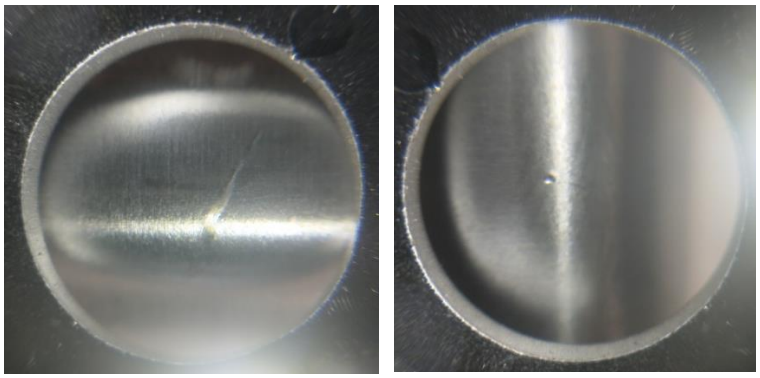

(a) Scratch (b) Point coordinates

Figure 3. Scratches and pitting occurred in the RF

Fig.4 shows the electron microscope observation of the inside of Zr alloy. As can be seen from Fig 4, the external structure of Zirconium alloy bar after corrosion is relatively flat, and the number of tiny holes is less, while the internal structure is relatively loose, and the number of tiny holes is more. Fig. 5 shows the internal and external observation results of Zirconium alloy rod, and the black spot morphology in the figure is the tiny hole after corrosion. As can be seen from Fig.5 (a), the number and size of micro-pores after external acid erosion of Zr alloy are small. As can be seen from Fig. 5 (b), the number and size of tiny holes eroded by acid solution inside the bar are large. This may be related to the way Zirconium alloy rods are processed [9-12].

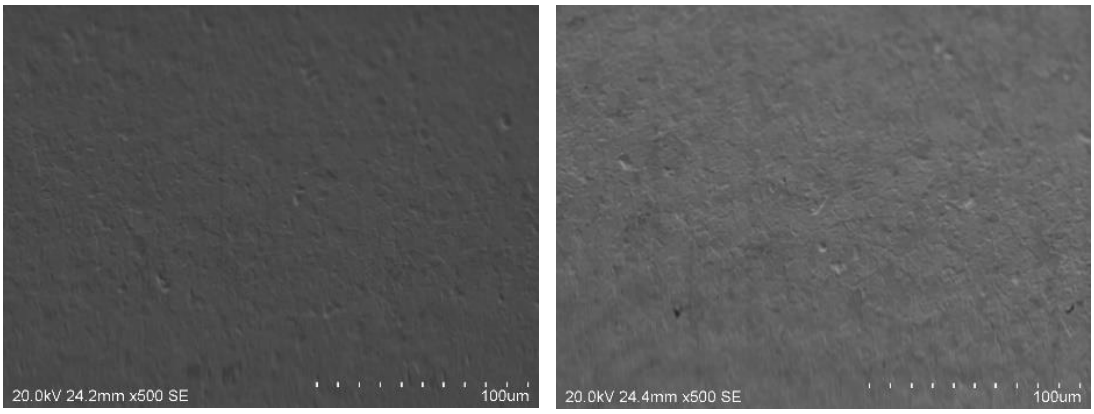

(a) external (b) internal

Figure 4. Internal and external electron microscope observation results of Zirconium alloy rods

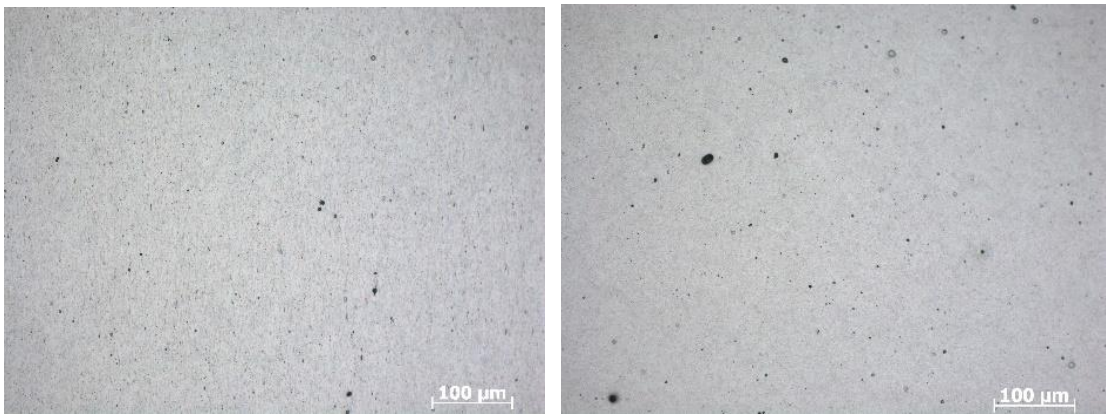

(a) external (b) internal

Figure 5. Observation results of internal and external metallographic structures of Zirconium alloy rods

Fig.6 shows the internal and external weave composition of Zirconium alloy bar. It can be seen from Fig6 that the (0002) surface of the grain inside and outside the Zirconium alloy bar is basically parallel to the rolling direction, indicating that there is a {0002} base texture inside and on the edge of the same bar end face. However, there is a significant difference between the inner and outer texture strength of the end face. The outer (0002) is concentrated at the central point, while the inner (0002) pole is approximately distributed in a ring around the vertical axis. If the {0002} crystal face is considered alone, the characteristic grain orientation diagram can be drawn, the outer (0002) crystal face axis rotates 360° around the rolling direction, forming a circular pole axis distribution diagram, while the inner (0002) crystal face axis is distributed vertically and radially from the center. It can be seen from the texture distribution in Figure 6 that there is rotational compressive stress on the outer end face of Zirconium alloy bar and compressive stress on the inner end face [13-15].

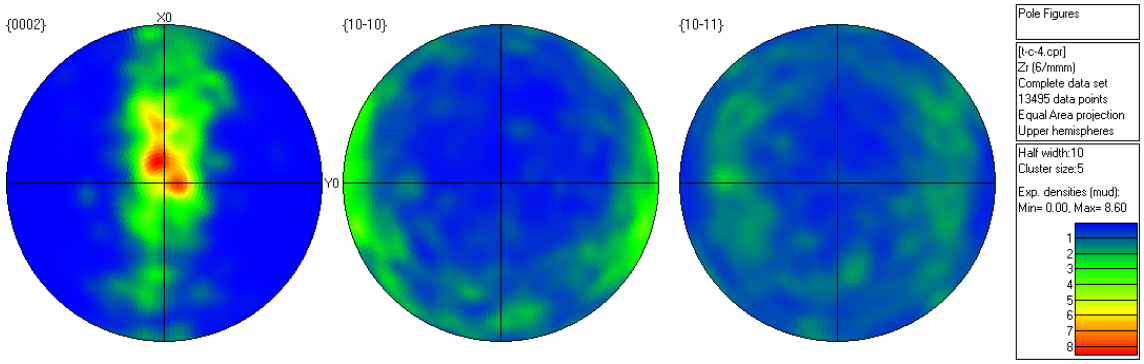

(a) External

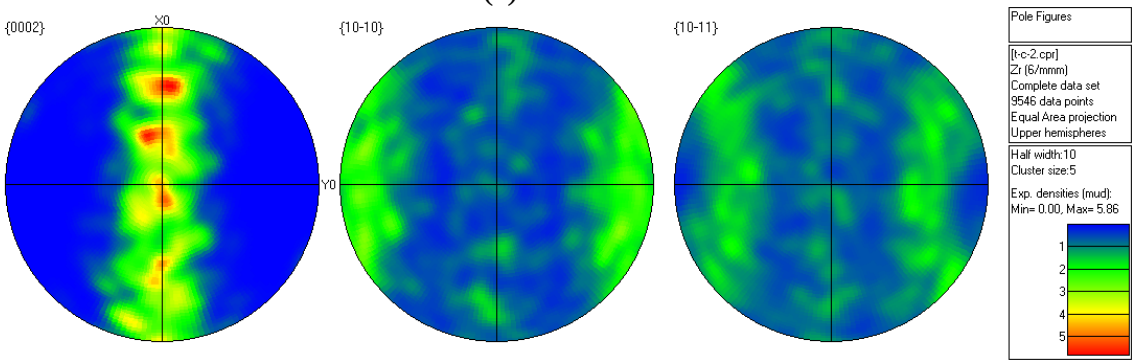

(b) Internally

Figure 6. Inner and outer end weave composition of Zr alloy rods

(2) Simulated result

In neural network [9-12], the objective of training is to find the set of weights and biases between the units that determine the global minimum of error function. If the network is properly trained, it has then learned to model the function that relates the input variables to the output variables and can subsequently be used to make predictions where the output is not known. This process is called testing and the ability of this network is called generalization. All the data are generally works best when the network inputs and targets are scaled so that they fall approximately in the range of 0 or 1. The operation principle and sample results are shown in Fig 7 and Table 1.

Table 1. The results of the sample data

	A	B	C	D	E
1-1	1	0	0	0	1
1-2	0	1	0	0	1
1-3	0	0	1	0	1
1-4	0	0	0	1	1
2-1	1	0	0	0	0
2-2	0	1	0	0	0
2-3	0	0	1	0	0
2-4	0	0	0	1	0

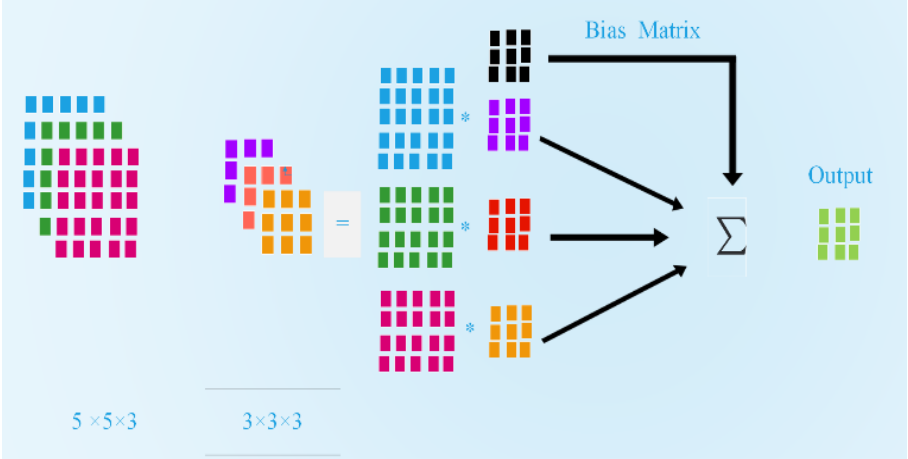

Figure 7. CNN operation

The CNN has been trained. The batch size is set to 8, the learning rate of the optimizer is set to 0.25, and the model training period is set to 200. The network structure and specific parameters of this chapter are shown in Table 2:

Table 2. Network structure and parameters

Layer	Output size	Size of conv kernel	Output channels	Stride
Input layer	256×256		3	
conv1	128×128	7×7	64	2
max pool	128×128	3×3	64	2
conv2_x	64×64	$\begin{bmatrix} 3\times & 3 \\ 3\times & 3 \end{bmatrix}\times 2$	$\begin{bmatrix} 64 \\ 64 \end{bmatrix}\times 2$	1
Conv3_x	32×32	$\begin{bmatrix} 3\times & 3 \\ 3\times & 3 \end{bmatrix}\times 2$	$\begin{bmatrix} 128 \\ 128 \end{bmatrix}\times 2$	1
Conv4_x	16×16	$\begin{bmatrix} 3\times & 3 \\ 3\times & 3 \end{bmatrix}\times 2$	$\begin{bmatrix} 256 \\ 256 \end{bmatrix}\times 2$	1
Conv5_x	5×5	$\begin{bmatrix} 3\times & 3 \\ 3\times & 3 \end{bmatrix}\times 2$	$\begin{bmatrix} 512 \\ 512 \end{bmatrix}\times 2$	1
Fc-6d	1×1		6	

The results show that the optimal network architecture is considered to be by GNN, which the Accuracy-Avg is 96%.

The model can also be used asa guide for to evaluate and predict the effect of RF which is in Fig 6. Fig. 6 is the FEM diagram of strain in the rolling process of Zirconium alloy bar. As can be seen from FIG. 6, at the beginning of rotary forging, the external surface of the Zirconium alloy bar is subjected to compressive stress by the rotary forging abrasive, and the external surface of the bar is the first to undergo plastic deformation. With the increase of rotary forging deformation, bar strain gradually increases and is gradually transferred from the outside to the inside [10-17]. The cold and hot processing of the bar can change the disordered polycrystalline material into a preferentially oriented material, and elongate the grain, so that the insoluble impurities and the second phase inside the material are deformed. Since the second phase and impurities of the grain are elongated into fibers along the main deformation direction of the metal, due to the inevitable existence of various impurities, second phase component segregation or casting defects in the metal, the formation of texture is a very common phenomenon in further processing. Due to the different deformation modes inside and outside the bar, there are certain differences in the texture of the inside and outside. Macroscopically, the outer part of the rolled bar is relatively dense, while the inner part is relatively loose. The above results are consistent with the internal and external electron microscope observation of the bar. In addition, after the corrosion of the bar, the external dense organization is not easy to corrosion, so the number of corrosion pits is small and the size is small, on the contrary, the number of corrosion pits in the relatively loose area inside is large and the size is larger.

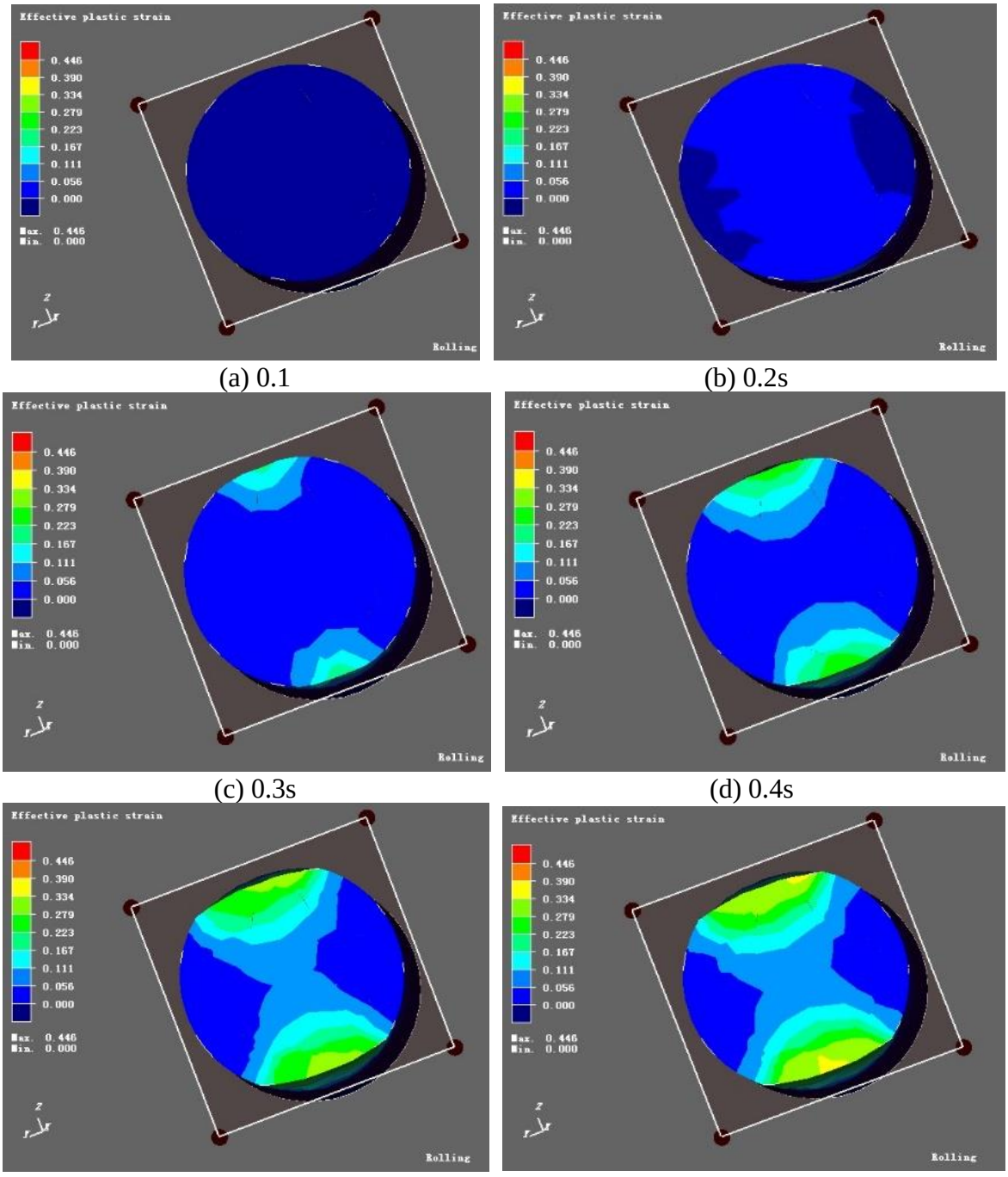

(a) 0.1 (b) 0.2s

(c) 0.3s (d) 0.4s

(e) 1s (f) 1.2s

Figure 8. FEM diagram of strain in RF of Zr alloy rods

5. Conclusion

The spinning forging process of Zirconium alloy bar was studied by combining experiment and simulation. The results show that:

(1) Point pits and scratches often occur in rotary forging. Modifying die size and increasing entrance Angle can effectively improve such defects as point pits and scratches.

(2) The external structure of Zirconium alloy bar is relatively dense, and the internal structure is relatively loose. The number and size of micro-holes after acid erosion are small. The number and size of the tiny holes after internal acid erosion are large.

(3) The (0002) planes of the inner and outer grains of the Zirconium alloy bar are basically parallel to the RF direction, but the outer (0002) is concentrated on the pole, and the inner (0002) pole is

approximately distributed in a ring around the longitudinal axis. As a result, there are differences in the small holes inside and outside the bar after corrosion

(4) The effect of resarch on the classification Method of RF in by GNN, which the Accuracy-Avg is 96%. At the beginning of RF, the rolled pass exerts compressive stress on the outside of the Zirconium alloybar, and the outside of the bar is the first to undergo plastic deformation. With the increase of RE deformation, the bar strain gradually increases and is gradually transferred from the outside to the inside.

References

[1] Qingle Meng, Lifeng Huang, Chunyang Bu. Genetic analysis of hollow fracturting thick molybdenum bires [J]. China Molybdenum Industry, 2013, 6: 43 - 46.

[2] Ming Luo, Jinglian Fan, Shiha Huang, et. all. Annealing behavior of rotary forging Mo-Ti-Zr alloy bars [J]. The Chinese Journal of Nonferrous Metals, 2010, Vol 20 (5): 866 - 871.

[3] Wei Hang, Kuiliu Gong, Shiha Huang, et, al. Effect of rotary forging on microstructure and properties of Cu-0.51Cr-0.06Zr alloy [J]. Ornance Material science and engineering, 2022, 45 (1): 83 - 88.

[4] Simonyan K, Zisserman A. Very Deep Convolutional Networks for Large-Scale Image Recognition [J]. Computer Science, 2014.

[5] Xue Xiangyi, Bai Xinde, Tian Zhenye et al. Study on Abnormal microstructure of cold rolled zirconium alloy bar for nuclear fuel rod end plug [J]. Rare Metals Sustainability and Engineering, 2004, 33 (8): 804 - 807.

[6] Qiu Jun, ZHAO Wenjin, Jiang Hongman, et al. Study on Properties of N36 Zirconium Alloy Bar [J]. Hot Working Technology, 2013, 42 (2): 79 - 83. (in Chinese).

[7] Wang Pengfei, Zhao Wenjin, Dai Xun. Study on texture of N36 zirconium alloy pipe [J]. Titanium Industry Progress,2016, 33 (3): 38 - 42.

[8] Liu Erwei, Zhang Xiyan, Chen Jianwei et al. Texture Analysis of rolled plates with Zr-Nb, Zr-Sn-Nb alloys [J]. 2012, 41 (2): 226 - 289.

[9] Chen Jianwei, Yu Hongbing, et al. Study on Texture evolution Model of Zr-Sn-Nb Alloy during Cold rolling [J]. 2013, 42 (11): 2279 - 2283.

[10] Luan Baifeng, Xiao Dongping, He Fangfang. Microstructure and texture evolution of pure zirconium during rolling [J]. Journal of Electron microscopy, 2012, 31 (6): 476 - 480. (in Chinese).

[11] Luan Baifeng, Ye Qing, Chen Jianfeng et.al. Deformation twinning and textural evolution of pure Zirconium during rolling at low temperature [J]. Journal of Nonferrous Science and Technology, 2013, 13: 2890 - 2895.

[12] Peng Qian, Shen Baobao. Texture of zirconium alloy and its effect on properties [J]. Rare Metals, 2005, 29 (6): 903 - 906. (in Chinese).

[13] Liu Hong, Dai Xun, Wang Ying et al. EBSD analysis of reprocessed microstructure of N18 zirconium alloy [J]. Journal of Electron Microscopy,2010, 29 (5): 437 - 441. (in Chinese).

[14] Nikolay Biba. QForm3d- New development of forging simulation [J]. The 9th China International Forging Exchange Conference, 2007: 157 - 170.

[15] He Wenwu, Liu Jiansheng, Guo Yinfang. Microstructure evolution and simulation of multi-fire forging of Mn18Cr18N protective ring steel [J]. Journal of Plasticity Engineering, 2010, 17 (2): 45 - 49.

[16] Yu Dejun, Bai Chunguang, Xu Dongsheng, et al. Finite element Simulation of titanium alloy opening forging Process [J]. The Chinese Journal of Nonferrous Metals, 2010, 20 (1): 500 - 504. (in Chinese).

[17] Si Jiayong, Han Pengbiao, Gao Fan et al. Numerical simulation of high temperature forging process of TiAl alloy [J], Materials Engineering, 2009, 3: 22 - 31.